Ammonia Decomposition Enhancement by Cs-Promoted Fe/Al$_2$O$_3$ Catalysts

Luke A. Parker[1,2] · James H. Carter[1] · Nicholas F. Dummer[1] · Nia Richards[1] · David J. Morgan[1] · Stanislaw E. Golunski[1] · Graham J. Hutchings[1]

Abstract

A range of Cs-doped Fe/Al$_2$O$_3$ catalysts were prepared for the ammonia decomposition reaction. Through time on-line studies it was shown that at all loadings of Cs investigated the activity of the Fe/Al$_2$O$_3$ catalysts was enhanced, with the optimum Cs:Fe being ca. 1. Initially, the rate of NH$_3$ decomposition was low, typically < 10% equilibrium conversion (99.7%@500°C) recorded after 1 h. All catalysts exhibited an induction period (typically ca. 10 h) with the conversion reaching a high of 67% equilibrium conversion for Cs:Fe = 0.5 and 1. The highest rate of decomposition observed was attributed to the balance between increasing the concentration of Cs without blocking the active site. Analysis of H$_2$-TPR and XPS measurements indicated that Cs acts as an electronic promoter. Previously, Cs has been shown to act as a promoter for Ru, where Cs alters the electron density of the active site, thereby facilitating the recombination of N$_2$ which is considered the rate determining step. In addition, XRD and N$_2$ adsorption measurements suggest that with higher Cs loadings deactivation of the catalytic activity is due to a layer of CsOH that forms on the surface and blocks active sites.

Graphic Abstract
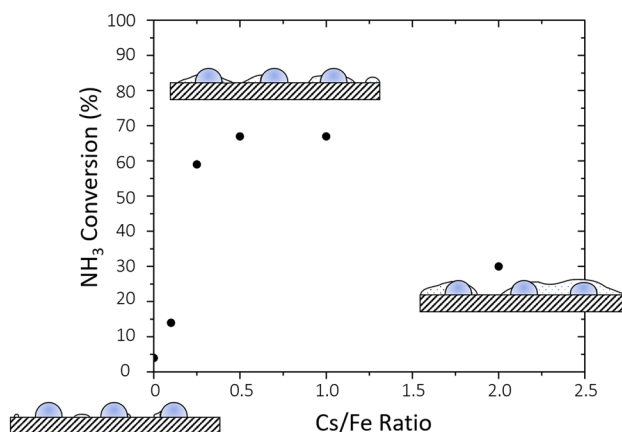
✉ Graham J. Hutchings
hutch@cardiff.ac.uk

1 Cardiff Catalysis Institute, School of Chemistry, Cardiff University, Cardiff CF10 3AT, UK

2 Present Address: Inorganic Chemistry and Catalysis, Debye Institute for Nanomaterials Science, Utrecht University, Universiteitsweg 99, 3584 CG Utrecht, The Netherlands

1 Introduction

In the fight against climate change caused by, among other contributors, the large amounts of CO$_2$ emitted through the burning of fossil fuels, the hydrogen economy has become a desirable and prominent field of research. A recent study by the Intergovernmental Panel on Climate Change (IPCC)

reported that the situation is more ominous than previously thought, with immediate and radical change necessary to stop the average global temperature increasing by 2 °C, accelerating the need for clean fuels [1]. An alternative to fossil fuel combustion for automotive applications is the use of proton exchange membrane fuel cells (PEMFC), which do not produce any CO_x by-products [2]. This has led to a renewed interest in the ammonia decomposition reaction, previously studied to gain insights into the synthesis reaction [3, 4], as a source of H_2 for fuel cells [5–7]. Hydrogen itself is limited by storage and transportation, requiring large storage tanks at pressures in excess of 200 bar, so alternative hydrogen sources have been widely investigated [8–11]. Traditional hydrogen sources such as methanol and methane reforming produce CO_x by-products which not only contribute to climate change but also poison the membranes of PEMFCs [12, 13]. Whilst ammonia is a potent poison itself (with tolerances < 1 ppm) [14] its removal by absorber or through use of a membrane reactor have been demonstrated to be highly effective [15, 16]. Ammonia can be liquefied at moderate pressures and at ambient temperatures enabling it to be stored easily on-board and making it compatible with the current liquid fuel infrastructure as well as presenting a renewable alternative for stationary power generators.

Alkali and alkaline earth metals have been demonstrated as promoters for Fe in the ammonia synthesis reaction [17, 18] and are well researched as promoters for Ru in the decomposition reaction [19, 20]. It has been shown that certain metals, such as Ba, act as structural promoters by assisting the formation of the most active phase of the metal whereas other metals, such as Cs, have been demonstrated to be electronic promoters [21]. K is also well-investigated as a promoter for the ammonia synthesis reaction, where it acts also acts as an electronic promoter [22].

Cs has previously been shown to act as a promoter for Fe in the NH_3 decomposition reaction [23], however, to our knowledge detailed studies into the optimisation of the promoter have not been reported. In this work, we investigate the optimal loading of Cs as a promoter for Fe/Al_2O_3 catalysts prepared through a simple co-impregnation technique. Through catalytic NH_3 decomposition testing an optimal Cs:Fe ratio of ca. 1 was observed, above which the decomposition rate is significantly supressed. Characterisation through XRD, XPS and N_2 adsorption show this suppression of the promotion effect to be due to the formation of a CsOH surface layer leading to less exposed Fe sites. However, under optimal conditions we demonstrate that Cs acts as an electronic promoter of Fe for NH_3 decomposition.

2 Experimental

2.1 Chemicals

Iron nitrate (Fe(NO$_3$)$_3$·9H$_2$O, ≥ 98%), Caesium Nitrate (CsNO$_3$, 99.99%) and γ-alumina (γ-Al$_2$O$_3$, nanopowder < 50 nm particle size) were purchased from Sigma Aldrich. 5000 ppm NH$_3$/Ar was purchased from BOC. All reagents were used as received.

2.2 Catalyst Preparation by Co-impregnation

Fe(NO$_3$)$_3$·9H$_2$O (5 wt%) and CsNO$_3$ (0.1, 0.25, 0.5, 1 and 2 mol eq. Cs) were dissolved in deionised water and stirred. Al$_2$O$_3$ was added and the resultant suspension was heated at 80 °C until the excess solvent was removed and a thick paste was formed. This paste containing the catalyst precursor was dried (110 °C, 16 h). The as-prepared catalyst was then reduced in a tube furnace at 550 °C for 3 h with a heat ramp of 10 °C/min under a flow of 5% H$_2$/Ar. The catalyst was tested immediately upon removal from the tube furnace to minimise re-oxidation in air.

2.3 Ammonia Decomposition Reactions

Catalytic testing was carried out on pelleted catalyst samples (300–425 μm) in a quartz, fixed-bed flow reactor (i.d.: 6 mm, catalyst mass: 100 mg) under a flow of dilute NH$_3$ (5000 ppm NH$_3$/Ar, 100 ml/min) at 500 °C. These conditions were chosen to be comparable with many previous literature studies and also as they allow for a comparison of all catalysts at the same temperature with no catalyst being limited by equilibrium or being completely inactive. Before the reaction, the catalyst was pre-treated under a flow of Ar (100 ml/min) at 500 °C for 1 h to remove any surface contaminants. On-line analysis of the effluent gas stream was carried out by Gasmet DX4000 Fourier-Transform Infra-red spectrometer (FT-IR) and the conversion was calculated after steady-state was achieved. Experimental error on this testing set-up has been determined as ± 2% through the triplicate testing of six different catalysts exhibiting conversions between 3 and 76%.

2.4 Characterisation

X-ray photoelectron spectroscopy (XPS) was carried out using a Thermo Fisher Scientific K-alpha + spectrometer. A monochromatic Al K$_α$ X-ray source was used to analyse the samples over an area of $600 × 400$ microns. Data was recorded at energies of 150 eV for survey scans and 40 eV

for high resolution scans with a step size of 0.1 eV. The neutralisation of charge was achieved through low energy electrons and argon ions.

XRD patterns were attainted by mounting samples in an in-situ cell under an N$_2$ flow and patterns were analysed using a Panalytical X'Pert diffractometer with a Cu X-ray source operating at 40 kV and 40 mA. Patterns were attained by 20 min scans over a range of 5–80° 2θ angles. Phase identification was performed by matching experimental patterns against entries from the International Centre for Diffraction Data (ICDD) database.

Temperature programmed reduction (TPR) was performed using a Quantachrome ChemBET Pulsar and the associated TPRWin software. 50 mg catalyst was fixed between two quartz wool plugs in the analysis tube and was pre-treated at 160 °C (20 °C/min heating rate) for 60 min under an Ar flow. Reduction of samples was then carried out using 10% H$_2$/Ar from room temperature to 600 °C with a heating rate of 5 °C/min.

Specific surface area measurements were carried out using a Quantachrome Quadrabsorb. Catalyst in the order of ca. 10 m^2 was degassed for 16 h at 250 °C before N$_2$ physisorption was performed at 77 K. Specific surface area was calculated using the BET equation with 5 points in the linear region 0.05–0.35 p/p$_0$.

3 Results and Discussion

Five Cs-promoted catalysts, referred henceforth by the molar ratio of Cs (e.g. 0.1Cs etc.), were prepared and tested for NH$_3$ decomposition at 500 °C for 24 h and compared to an unpromoted Fe catalyst, as shown in Fig. 1a. The unpromoted catalyst exhibits a low conversion of 4% across the 24 h tested, however, all Cs-promoted catalysts show an enhancement in activity confirming the use of Cs as a promoter, with the highest conversions achieved being ca. 70%. This is a vast improvement over the unpromoted catalyst, however it is still some way short of the equilibrium conversion of 99.7% for this temperature (500 °C). It is interesting to note that all promoted catalysts exhibited induction periods, however, these varied with Cs loading. Previous Cs-promoted studies reported that Cs was present in the hydroxide form, CsOH [20]. Compounds of Cs are known to have low melting points (CsOH = 272 °C, Cs$_2$O = 490 °C) and therefore at the reaction temperature (500 °C) are likely to exhibit surface mobility. This sort of mobility is well-known for other alkali metal promoters such as K [24]. As contact between the promotor and active metal is required for electronic promotion on a non-conducting support such as Al$_2$O$_3$, we consider that during this period the mobility of Cs can allow it to disperse over the catalyst surface, contacting more Fe and thus creating more promoted Fe sites. Although all care was taken to minimise air exposure and transfer time between catalyst reduction in a tube furnace and testing, it
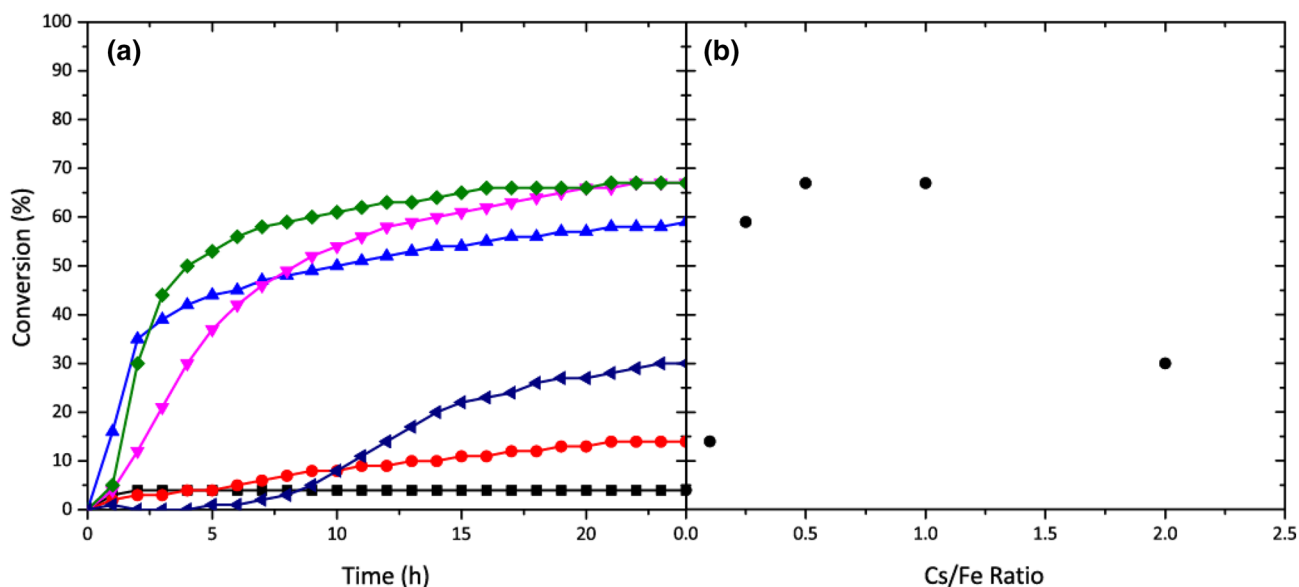
Fig. 1 a Time on-line results for the Cs-promoted Fe catalysts: 0.1Cs (filled circle), 0.25Cs (filled triangle), 0.5Cs (inverted filled triangle), 1Cs (filled diamond) and 2Cs (left filled triangle); and Fe (0Cs, filled square). **b** Effect of Cs loading on ammonia decomposition activity at 24 h time-on-line. Conditions for both: 100 ml/min 5000 ppm NH$_3$/Ar, 100 mg$_{catalyst}$, 500 °C. Equilibrium conversion at this temperature is 99.7%

is also possible that some Fe became re-oxidised. Therefore, another contribution to this induction period may be the reduction of Fe by H_2 produced in the reaction, thus creating more active sites and increasing activity. In order to compare these catalysts, the conversion after 24 h, when all catalysts had reached a steady-state conversion, was used and is shown in Fig. 1b.

Initially, increasing the Cs concentration leads to an enhancement in activity, however, at Cs:Fe > 1, the activity enhancement is diminished. It can be seen that the optimal Cs:Fe ratio lies between 0.5 and 1 due to the catalysts exhibiting similar conversion at 24 h. This can be reasoned by a balance between the enhancing properties of Cs and by an inhibiting effect caused by excess Cs, as seen with the 2Cs sample. When an 11 wt% Cs/Al_2O_3 catalyst (i.e. equivalent to Cs:Fe = 1) without Fe was tested it exhibited no activity, consistent with previous literature [20].

To investigate the active form of the catalyst, post-reaction samples were analysed by XRD, XPS and N_2-adsorption analysis. To minimise any changes in the post-reaction samples they were removed from the reaction tube in a glovebox and stored under a N_2 atmosphere.

XRD was performed on post-reaction samples under a N_2 atmosphere in an in-situ XRD cell and diffraction patterns are shown in Fig. 2. Six reflections are present at 32, 37, 39, 47, 62 and 68°2θ corresponding to γ-Al_2O_3 [25] and are due to the (220), (311), (222), (400), (333) and (440) planes of Al_2O_3 respectively [26]. No Fe or Fe_xO_y phases were observed in any sample. Given that the expected Fe phases (Fe^0, FeO, Fe_2O_3) are crystalline indicates that these are present below the detection limit (~ 4 nm) of the technique. From this we can say that the co-impregnation method used
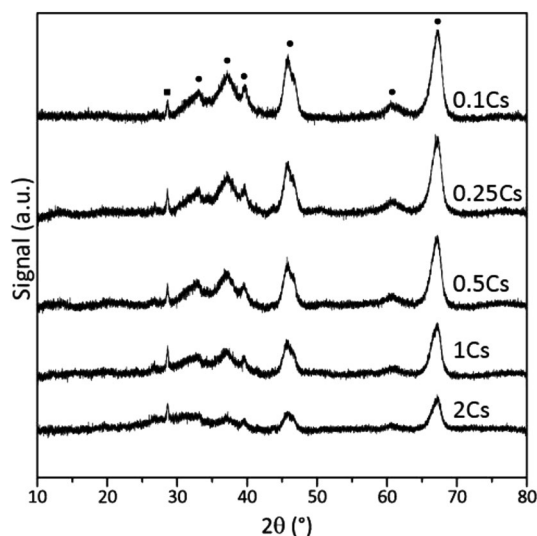
has produced well-dispersed and small Fe nanoparticles that maintain their dispersion and do not agglomerate to a large extent (indeed not above the detection limit) under 24 h of reaction conditions. The small, sharp peak at 29°2θ is due to the sample holder of the in-situ instrument. As the Cs-content of the catalysts increases the γ-Al_2O_3 reflections become weaker, with the 32° 2θ and 62° 2θ reflections being indefinable in the 2Cs catalyst. This suggests that an amorphous layer is forming on top of the support and attenuating the reflections of the Al_2O_3 support, as has been observed by TEM previously [27]. Cs has a high mass attenuation coefficient and as such absorbs X-ray radiation readily. As the Cs content of the catalyst increases and the CsOH layer grows thicker, more diffracted X-rays would be scavenged leading to the weaker reflections observed.

N_2-adsorption measurements were taken and the specific surface area was calculated using the BET equation as shown in Table 1. The addition of a low concentration of Cs has a negligible effect on the surface area, however at Cs:Fe > 1 the surface area decreased significantly, with the surface area of the 2Cs catalyst being almost half that of the Al_2O_3 support. This supports the analysis of the XRD data, that an amorphous layer of CsOH forms which blocks pores and lowers surface area. The modest increase in surface area for the 0.5Cs catalyst could be due to an increase in surface roughness due to islands of CsOH on the Fe/Al_2O_3.

The characterization by N_2-adsorption and XRD suggests that the inhibition of Cs-doped Fe/Al_2O_3 at Cs:Fe > 1 is due to the growth of a CsOH layer that blocks active sites. This is in agreement with the results observed by Hill et al. for Cs-promoted Ru catalysts. Using the conversion at 500 °C after 24 h the surface normalized activity was calculated and is also shown in Table 1. Again this shows that activity initially increases with increasing Cs concentration, however, when normalised for surface area the 1Cs catalyst (105.4 $mmol_{NH_3}$ m^{-2} h^{-1}) is ca. 20% more active than the 0.5Cs catalyst (82.0 $mmol_{NH_3}$ m^{-2} h^{-1}) and this was not evident from time-on-line data. When normalized for the lower surface area, the 2Cs catalyst (75.5 $mmol_{NH_3}$ m^{-2} h^{-1}) is still one of the least active catalysts, again demonstrating that

Fig. 2 XRD patterns of Cs-promoted Fe catalysts. Al_2O_3 reflections are indicated by filled circle and the reflection labelled with a filled square is due to the sample holder

Table 1 Post reaction BET surface area and surface normalised activity at 24 h T.O.L. for Cs-promoted Fe/Al_2O_3 catalysts

| Catalyst	Surface Area (m^2/g)	Conversion after 24 h (%)	Activity mol$_{NH_3}$ m^{-2} h^{-1}
Al_2O_3	124	0	n/a
0.1Cs	122	14	20.2
0.25Cs	129	59	80.6
0.5Cs	144	67	82.0
1Cs	112	67	105.4
2Cs	70	30	75.5

the Cs concentration must be carefully balanced between enhancing activity without blocking active sites.

X-Ray photoelectron spectroscopy was used to investigate the state of both Fe and Cs in the samples. Figure 3 illustrates Cs 3d and Fe 2p/3 regions of the XPS spectrum. The large peak at 724.0 eV is attributed to CsOH which confirms the assumption from XRD data that the majority of the Cs is present as an amorphous hydroxide phase. The intensity of the peak increases as the Cs concentration increases, as expected. It is important to note that although care was taken to minimise contact of post-reaction samples with air, this does occur for a brief period during XPS sample mounting and may have an effect on sample speciation. The broad peak between 705 and 715 eV is due to two Fe species; FeO (708.7 eV) and Fe$_2$O$_3$ (710.7 eV) are shown in the highlighted section of Fig. 3. As XPS is a surface sensitive technique, this data can also give information on the composition of the reactive surface of the catalysts. As the Cs concentration increases the Fe signal decreases in intensity. This is further illustrated by the ratio of Cs:Fe as shown in Table 2 where the observed ratio is much higher than calculated in all samples. Even in the 0.1Cs catalyst, with the lowest promoter concentration, the observed Cs:Fe is 0.4, 4× higher than expected. The 0.25Cs and 0.5Cs catalysts also have an observed Cs:Fe of ca. 4× higher than expected (1.2 and 1.9, respectively) and in the higher Cs catalysts, 1Cs and 2Cs the observed Cs:Fe is ca. 3× higher (3.4 and 6.2, respectively). This

Table 2 Ratios of expected and observed Cs and Fe species calculated from the XPS data in Fig. 3

Catalyst	Calculated Cs:Fe	Observed Cs:Fe	Cs:Al	FeO:Fe$_2$O$_3$
0.1Cs	0.1	0.4	0.02	0.12
0.25Cs	0.25	1.2	0.05	0.18
0.5Cs	0.5	1.9	0.10	0.18
1Cs	1	3.4	0.12	0.20
2Cs	2	6.2	0.27	0.36

demonstrates that due to the Cs covering the catalyst and lowering the surface area, there is less exposed Fe accessible for the reaction and this leads to the decrease in activity at higher concentrations. We consider that the lack of exposed Fe sites has a much greater effect than the loss of surface area in general and this is supported by the data in Table 1 that shows that despite the 1Cs catalyst having the second lowest surface area it has the joint highest conversion (and consequently the highest surface normalised activity). This also illustrates the need for a balanced promoter loading, as contact between promoter and active metal are required for the electronic promotion (as is discussed further on), however, this contact also reduces exposed active metal surface. The Cs:Al ratio is also presented and increases with Cs concentration from 0.02 to 0.27, demonstrating that the support is covered by
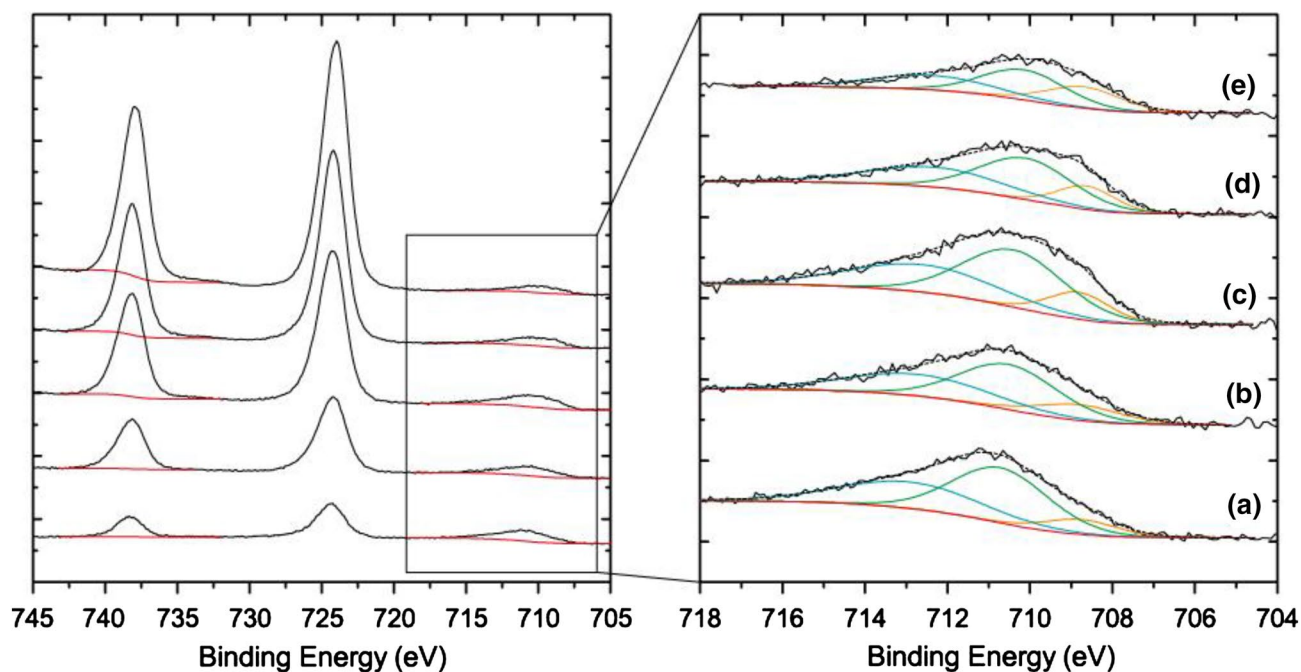

Fig. 3 (Left) The Cs 3d and Fe 2p/3 regions of the XP spectrum and Right) A zoom-in of the Fe 2p/3 region for (a) 01.Cs (b) 0.25Cs (c) 0.5Cs (d) 1Cs (e) 2Cs. Deconvoluted based on three Fe species: Fe^0 (yellow), FeO (green) and Fe$_2$O$_3$ (blue)

progressively more Cs and further supporting the formation of a CsOH layer as observed XRD and BET.

Table 2 shows that the FeO:Fe$_2$O$_3$ ratio increases with Cs concentration and suggests an electronic interaction between the Cs and Fe, as we consider the presence of Cs enhances the reduction of Fe. Previously, it has been shown that Cs acts as an electronic promoter for CNT supported Ru for this reaction [20].

H$_2$-TPR was performed on three promoted catalysts along with the unpromoted Fe catalyst and the Cs/Al$_2$O$_3$ sample (Fig. 4). These catalysts were prepared in the same way as the tested catalysts however they were not subjected to the reduction step in a tube furnace. Analysis of the resultant TPR profile of the unpromoted Fe catalyst shows H$_2$ uptake from ca. 250 °C with a maximum at 315 °C and the supported Cs sample shows a reduction peak at ca. 490 °C. However, the Cs-Fe catalysts exhibit only a broad reduction peak where the peak maxima increases with reduction temperature. The onset of this reduction peak remains at ca. 250 °C indicating that the reducibility of the Fe is not modified but that the Fe, once reduced, facilitates the reduction of the Cs. This could be due to the ability of metallic Fe to dissociate H$_2$ which can subsequently spillover to Cs [28]. A similar "facilitated reduction" phenomenon has been observed for Cs-promoted Ru catalysts reported previously [19]. This spillover mechanism also demonstrates that the Fe and Cs are in intimate contact with each other which would be required for electronic promotion by the Cs as will be described in detail further on. As the concentration of Cs increases, the reduction peaks shift to higher temperatures, due to less exposed Fe from which hydrogen spillover can occur, this is consistent with the XPS findings. The hydrogen uptake also increases as shown in Table 3 due to the higher concentration of Cs.
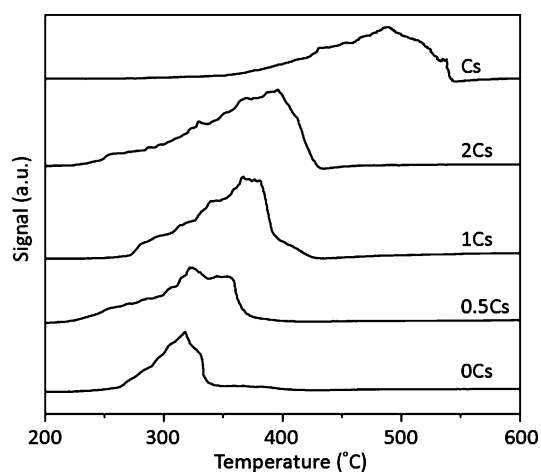
Fig. 4 H$_2$-TPR profiles of unpromoted Fe (0Cs), promoted Fe (0.5Cs, 1Cs and 2Cs) and Fe-free (Cs) catalysts

Table 3 Reduction temperatures and the hydrogen uptake per gram of catalyst for the catalysts derived from the H$_2$-TPR illustrated in Fig. 4

Catalyst	Reduction temp. (°C)	H$_2$ Uptake (μmol g^{-1})
Fe/Al$_2$O$_3$	315	1.47
Fe/Al$_2$O$_3$-0.5Cs	340	2.22
Fe/Al$_2$O$_3$-1Cs	360	3.14
Fe/Al$_2$O$_3$-2Cs	395	3.78
Cs/Al$_2$O$_3$	490	3.24

The promotional effect of alkali metals on supported metal nanoparticle catalysts has been widely studied and it is generally accepted that they function as chemical promoters, as opposed to structural promoters [20, 21]; that is they work by altering the reactive species on the active metal and not by stabilising a certain facet or site of said metal nanoparticle. This promotional mechanism has been studied in detail via a number of model studies as it is also common in large-scale industrial processes such as the Fischer–Tropsch reaction and it has been shown that when in contact with the metal, the alkali metal becomes polarised, leading to a dipole moment on the active metal which alters the chemistorption of reactants or intermediates with respect to the unpromoted metal [29]. In the context of the ammonia decomposition reaction, this weakens the adsorbed N* species on the metal and subsequently facilitates its recombinative desorption, which has been shown to be the rate-determining step, thus enabling an efficient turnover of active sites and therefore increasing the rate of reaction. The mobility of Cs that was previously suggested as a cause of the observed induction period is also a well-known phenomenon for alkali promoted catalysts. Potassium, which is commonly used as a catalyst promoter in both ammonia synthesis and Fischer–Tropsch procesess is understood to be mobile, subsequently it is lost over time in industrial-scale processes [24, 30]. Consequently, these catalysts require re-activation during their lifetime. Given that the melting point of Cs^0 as well as its oxides being lower than those of K, it is reasonable to expect that these same phenomena will be observed in this system over a prolonged period of testing. This electronic effect may only exist under reaction conditions as XPS and H$_2$-TPR measurements indicated that the presence of Cs enhances Fe reduction. However, the modification of the oxidation state of Fe in the presence of Cs confirms the interacton between the two supported phases and the origin of the observed increase in catalyst performance. The lowered Cs reduction temperature due to hydrogen spillover from the Fe demonstrates the intimate contact between Fe and Cs that is required for this promotional mechanism.

4 Conclusions

The remarkable activity enhancements of Fe/Al$_2$O$_3$ catalysts with the addition of Cs were demonstrated. The optimal Cs loading was found to be where Cs:Fe = ca. 1. Below this, activity is lower due to a less effective promotional effect, however, above this value activity decreases due to the formation of a surface layer of amorphous CsOH and lowers the catalyst surface area. TPR and XPS measurements demonstrated that Cs acts as an electronic promoter and significantly increases the catalytic activity. This was ascribed to a donation of electron density to Fe, which facilitated desorption of adsorbed N* species. Interestingly, a long induction period was observed in some samples, which was ascribed to mobile Cs on the surface of the catalyst.

References

1. IPCC (2018) Summary for policymakers of IPCC special report on global warming of 1.5°C approved by governments. IPCC, Geneva
2. Mehta V, Cooper JS (2003) Review and analysis of PEM fuel cell design and manufacturing. J Power Sources 114:32–53. https://doi.org/10.1016/S0378-7753(02)00542-6
3. Ozaki A, Taylor H (1960) Kinetics and mechanism of the ammonia synthesis. Proc R Soc A Math Phys Eng Sci 258:47–62. https://doi.org/10.1098/rspa.1960.0174
4. Love KS, Emmett PH (1941) The catalytic decomposition of ammonia over iron synthetic ammonia catalysts. J Am Chem Soc 63:3297–3308. https://doi.org/10.1021/ja01857a019
5. Durbin DJ, Malardier-Jugroot C (2013) Review of hydrogen storage techniques for on board vehicle applications. Int J Hydrogen Energy 38:14595–14617. https://doi.org/10.1016/j.ijhydene.2013.07.058
6. Yin SF, Xu BQ, Zhou XP, Au CT (2004) A mini-review on ammonia decomposition catalysts for on-site generation of hydrogen for fuel cell applications. Appl Catal A Gen 277:1–9. https://doi.org/10.1016/j.apcata.2004.09.020
7. Choudhary TV, Sivadinarayana C, Goodman DW (2001) Catalytic ammonia decomposition: COx-free hydrogen production for fuel cell applications. Catal Letters 72:197–201
8. Joó F (2008) Breakthroughs in hydrogen storage-formic acid as a sustainable storage material for hydrogen. Chemsuschem 1:805–808. https://doi.org/10.1002/cssc.200800133
9. Rosi NL, Eckert J, Eddaoudi M et al (2003) Hydrogen storage in microporous metal-organic frameworks. Science 300:1127–1129. https://doi.org/10.1126/science.1083440
10. Eberle U, Felderhoff M, Schüth F (2009) Chemical and physical solutions for hydrogen storage. Angew Chem Int Ed 48:6608–6630. https://doi.org/10.1002/anie.200806293
11. Sakintuna B, Lamari-Darkrim F, Hirscher M (2007) Metal hydride materials for solid hydrogen storage: a review. Int J Hydrogen Energy 32:1121–1140. https://doi.org/10.1016/j.ijhydene.2006.11.022
12. Yin S-F, Zhang Q-H, Xu B-Q et al (2004) Investigation on the catalysis of COx-free hydrogen generation from ammonia. J Catal 224:384–396. https://doi.org/10.1016/j.jcat.2004.03.008
13. Choudhary T (2002) CO-free fuel processing for fuel cell applications. Catal Today 77:65–78. https://doi.org/10.1016/S0920-5861(02)00233-X
14. Engstr A (2014) Determination of acceptable contaminant levels for PEM fuel cell stacks and poisoning mitigation strategies. PhD Thesis
15. García-García FR, Ma YH, Rodríguez-Ramos I, Guerrero-Ruiz A (2008) High purity hydrogen production by low temperature catalytic ammonia decomposition in a multifunctional membrane reactor. Catal Commun 9:482–486. https://doi.org/10.1016/j.catcom.2007.07.036
16. Chellappa A, Fischer C, Thomson W (2002) Ammonia decomposition kinetics over Ni-Pt/Al$_2$O$_3$ for PEM fuel cell applications. Appl Catal A Gen 227:231–240. https://doi.org/10.1016/S0926-860X(01)00941-3
17. Rayment T, Schlögl R, Thomas JM, Ertl G (1985) Structure of the ammonia synthesis catalyst. Nature 315:311–313. https://doi.org/10.1038/315311a0
18. Ertl G, Lee SB, Weiss M (1982) Adsorption of nitrogen on potassium promoted Fe(111) and (100) surfaces. Surf Sci 114:527–545. https://doi.org/10.1016/0039-6028(82)90703-8
19. Hill AK, Torrente-Murciano L (2015) Low temperature H2 production from ammonia using ruthenium-based catalysts: synergetic effect of promoter and support. Appl Catal B Environ 172–173:129–135. https://doi.org/10.1016/j.apcatb.2015.02.011
20. Hill AK, Torrente-Murciano L (2014) In-situ H2 production via low temperature decomposition of ammonia: Insights into the role of cesium as a promoter. Int J Hydrogen Energy 39:7646–7654. https://doi.org/10.1016/j.ijhydene.2014.03.043
21. Kowalczyk Z, Krukowski M, Raróg-Pilecka W et al (2003) Carbon-based ruthenium catalyst for ammonia synthesis: Role of the barium and caesium promoters and carbon support. Appl Catal A Gen 248:67–73. https://doi.org/10.1016/S0926-860X(03)00150-9
22. Strongin DR, Somorjai GA (1988) The effects of potassium on ammonia synthesis over iron single-crystal surfaces. J Catal 109:51–60. https://doi.org/10.1016/0021-9517(88)90184-4
23. Li Y, Yao L, Liu S et al (2011) Cs-modified iron nanoparticles encapsulated in microporous and mesoporous SiO2 for COx-free H2 production via ammonia decomposition. Catal Today 160:79–86. https://doi.org/10.1016/J.CATTOD.2010.02.066
24. Connell G, Dumesic JA (1985) Migration of potassium on iron and alumina surfaces as studied by Auger electron spectroscopy. J Catal 92:17–24. https://doi.org/10.1016/0021-9517(85)90233-7
25. Rozita Y, Brydson R, Scott AJ (2010) An investigation of commercial gamma-Al$_2$O$_3$ nanoparticles. J Phys Conf Ser 241:012096. https://doi.org/10.1088/1742-6596/241/1/012096
26. Lippens BC, de Boer JH (1964) Study of phase transformations during calcination of aluminum hydroxides by selected area

electron diffraction. Acta Crystallogr 17:1312–1321. https://doi.org/10.1107/S0365110X64003267

27. Larichev YV, Shlyapin DA, Tsyrul'nikov PG, Bukhtiyarov VI (2008) Comparative study of rubidium and cesium as promoters in carbon-supported ruthenium catalysts for ammonia synthesis. Catal Lett 120:204–209. https://doi.org/10.1007/s10562-007-9270-y

28. O'Byrne JP, Owen RE, Minett DR et al (2013) High CO_2 and CO conversion to hydrocarbons using bridged Fe nanoparticles on carbon nanotubes. Catal Sci Technol 3:1202. https://doi.org/10.1039/c3cy20854k

29. Bonzel HP (1987) Alkali-metal affected adsorption of molecules on metal surfaces. Surf Sci Rep 8:43–125

30. Niemantsverdriet JW (2007) Case studies in catalyst characterization. In: Spectroscopy in catalysis. Wiley-VCH Verlag GmbH & Co. KGaA, Weinheim, pp 251–295